

# Radiative Capture Reaction $d(\alpha, \gamma)^6\text{Li}$ in Cluster Effective Field Theory

F. Nazari\* and M. Radin†

*Department of Physics, K. N. Toosi University of Technology, P.O.Box 16315-1618, Tehran, Iran*

M. Moeini Arani‡

*Malek Ashtar University of Technology, Tehran, Iran*

In this study, we focus on the radiative capture process of the deuteron on alpha particle leading to the formation of  $^6\text{Li}$  in the two-body formalism through the cluster effective field theory (CEFT). It was the primitive nuclear reaction to produce  $^6\text{Li}$  in a few minutes after the Big Bang. In detail, we outline the calculation of the dominant  $E1$  and  $E2$  electromagnetic transition amplitudes of  $d(\alpha, \gamma)^6\text{Li}$ . Then, we obtain the astrophysical S-factor by fitting it to the experimental data. Finally, we compare the obtained CEFT results for the astrophysical S-factor with the other theoretical results.

**Keywords.** Cluster Effective Field Theory, Gamma Capture Reaction, Electromagnetic Transition, Astrophysical S-factor

**PACS.** 21.45.-v Few-body systems - 11.10.-z Field theory - 23.20.-g Electromagnetic transitions.

## I. INTRODUCTION

In the standard Big Bang Nucleosynthesis (BBN) framework, the primitive  $^6\text{Li}$  abundance is mainly determined by two nuclear reactions. The  $d(\alpha, \gamma)^6\text{Li}$  reaction where deuteron reacts with an alpha particle to produce  $^6\text{Li}$ . This reaction leads to the formation of  $^6\text{Li}$  during the primordial nucleosynthesis process [1, 2]. Conversely, the  $^6\text{Li}(p, \alpha)^3\text{He}$  reaction that can destroy  $^6\text{Li}$ . In this reaction, the  $^6\text{Li}$  reacts with a proton to produce an alpha particle and

---

\*Electronic address: [f.nazari@email.kntu.ac.ir](mailto:f.nazari@email.kntu.ac.ir)

†Electronic address: [radin@kntu.ac.ir](mailto:radin@kntu.ac.ir)

‡Electronic address: [m.moeini.a@ut.ac.ir](mailto:m.moeini.a@ut.ac.ir)

$^3\text{He}$ . This reaction reduces the abundance of  $^6\text{Li}$  in the early universe. This reaction rate is commonly understood within the BBN energy range and has been extensively researched using various techniques [3–7].

Consequently, the  $^6\text{Li}$  production reaction has recently been a prime focus of studies, both experimentally and theoretically [8–17]. The available experimental data for this reaction cover the region  $0.1 \text{ MeV} \leq E_{CM} \leq 4 \text{ MeV}$  [1, 18–22]. The low-energy experimental data have been obtained indirectly from measurements using the Coulomb breakup process  $^6\text{Li} + ^{208}\text{Pb} \rightarrow \alpha + d + ^{208}\text{Pb}$  [21]. The most historical theoretical calculations of the low energy cross section for the reaction has been performed within the framework of the microscopic resonating group method, in the quasi-microscopic potential model, and the framework of the multicluster dynamic model [23–25].

In this study, we concentrate on utilizing the cluster effective field theory (CEFT) as one of the most precise techniques for low-energy nuclear processes for the investigation of gamma capture reaction  $d(\alpha, \gamma)^6\text{Li}$ . The CEFT is the ideal tool for analyzing the features of halo states with minimal assumptions [26, 27]. It describes systems through their effective degrees of freedom, i.e., core and valence nucleons, with interactions governed by low-energy constants. The cluster EFT was formulated in the study of the shallow p-wave neutron-alpha resonance and applied to other systems, such as the s-wave alpha-alpha resonance, electromagnetic transitions, and capture reactions. In this paper, we apply this idea to the  $d(\alpha, \gamma)^6\text{Li}$  radiative reaction, following a cluster approach of point-like objects. Our investigation leads to calculating the astrophysical S-factor of the mentioned reaction.

The manuscript is organized as follows: In Sec. II, The possible and dominant electromagnetic transition of the  $d(\alpha, \gamma)^6\text{Li}$  reaction was introduced. Moreover, The effective non-relativistic lagrangian of the system was presented which concluded the scattering and additional terms for the radiative capture process. The details of the Coulomb interaction were investigated in this section. Sec. III is dedicated to the basic feature of the elastic scattering  $d(\alpha, \alpha)d$  reaction in CEFT. In the following section, Sec. IV, we review the principles of radiative capture reaction. Furthermore, we derive relevant expressions for the capture amplitude and cross-section for the  $E1$  and  $E2$  transitions in this section. Sec. V collects the numerical results, in particular, the astrophysical S-factor. Our concluding remarks are presented in Sec. VI.

## II. RADIATIVE CAPTURE REACTION

In this section, we first discuss the possible and most prevalent electromagnetic transitions that occur during the radiative capture process of  $d(\alpha, \gamma)^6\text{Li}$  at low energies. Then, we present the Lagrangian of this reaction based on two-body CEFT. From a schematic point of view, in a radiative capture reaction, a stationary nucleus in a definite quantum mechanical state makes a transition to a lower energy state via the emission of a single photon. The conservation of angular momentum plays a controlling role in the gamma ray decay process. Both the initial and final states of the nucleus will possess a precise angular momentum and parity, necessitating the photon to connect these two states while preserving both parity and angular momentum. Photons carry a precise amount of angular momentum and possess a specific parity, with the conservation of these properties influencing the characteristics of the emitted photon. The electromagnetic selection rules and multipolarities for nuclear physics are outlined in Table. I.

TABLE I: The electromagnetic selection rules.  $\Delta l$  and  $\Delta\pi$  are angular momentum and parity of the photon.

Radiation Type	Name	$\Delta l$	$\Delta\pi$
$E1$	Electric dipole	1	yes
$M1$	Magnetic dipole	1	no
$E2$	Electric quadrupole	2	no
$M2$	Magnetic quadrupole	2	yes

Generally, the likely type of photon involved in a transition between nucleus can be determined by considering the properties of photons. First, the parity of the photon ( $\Delta\pi$ ) is determined by the difference in parities of the two nuclear states. The photon angular momentum is then constrained within the range of  $|l_i - l_f| \leq \Delta l \leq l_i + l_f$ , where  $l_f$  and  $l_i$  are the angular momentums of the final and initial states of the nucleus, respectively. The multipolarity of the photon is specified by the amount of angular momentum carried by the photon [28].

Considering the spin-zero and spin-one of the alpha and deuteron respectively, and taking

into account the  $l$ -wave of the  $d - \alpha$  system, the possible incoming states corresponding to the relevant total angular momenta  $j = 0, 1, 2, 3$ , are  $\xi = {}^3S_1, {}^3P_0, {}^3P_1, {}^3P_2, {}^3D_1, {}^3D_2, {}^3D_3$  [29]. The final ground state of the  ${}^6\text{Li}$  nucleus with  $J^\pi = 1^+$ , is  ${}^3S_1$ . According to the electromagnetic transition rules of nuclear physics, the  $E1$  and  $E2$  transitions contribute to the  $d(\alpha, \gamma){}^6\text{Li}$  radiative capture amplitude in the low-energy regime. Transitions from  $P$ -waves to  $S$ -wave, which changes parity and results in an angular momentum change of  $\Delta l = 1$ , are considered  $E1$  transitions. Transitions from  $D$ -waves to  $S$ -wave, which do not change parity but involves an angular momentum change of  $\Delta l = 2$ , contribute to the  $E2$  transition. Therefore, the possible electromagnetic transitions during the radiative capture process in the  $d(\alpha, \gamma){}^6\text{Li}$  reaction at low energies can be outlined as follows

$${}^3P_0, {}^3P_1, {}^3P_2 \xrightarrow{E1} {}^3S_1, \quad {}^3D_1, {}^3D_2, {}^3D_3 \xrightarrow{E2} {}^3S_1.$$

### A. Effective Lagrangian

In this work, the deuteron and alpha are considered as point-like particles. Therefore, in the CEFT that we construct for the  $d - \alpha$  system, the degrees of freedom are the deuteron and alpha particles, and the  ${}^6\text{Li}$  nucleus treats as a bound state of point-like nuclear clusters alpha and deuteron with a binding energy  $B = 1.47$  MeV. The effective non-relativistic Lagrangian which describes the dynamics in all possible channels  $\xi$ , can be written as

$$\mathcal{L}^{[\xi]} = \mathcal{L}_{ES}^{[\xi]} + \mathcal{L}_{RC}^{[\xi]}, \quad (1)$$

where  $\mathcal{L}_{ES}^{[\xi]}$  defines the elastic scattering and  $\mathcal{L}_{RC}^{[\xi]}$  denotes the additional terms for the radiative capture process. The Lagrangian  $\mathcal{L}_{ES}^{[\xi]}$  is given by [30]

$$\begin{aligned} \mathcal{L}_{ES}^{[\xi]} = & \phi^\dagger \left( i\partial_0 + \frac{\nabla^2}{2m_\alpha} \right) \phi + d_i^\dagger \left( i\partial_0 + \frac{\nabla^2}{2m_d} \right) d_i + \eta^{[\xi]} t^{[\xi]\dagger} \left[ i\partial_0 + \frac{\nabla^2}{2m_t} - \Delta^{[\xi]} \right] t^{[\xi]} \\ & + g^{[\xi]} [t^{[\xi]\dagger} (\phi \Pi^{[\xi]} d) + h.c.] + h^{[\xi]} t^{[\xi]\dagger} \left[ \left( i\partial_0 + \frac{\nabla^2}{2m_t} \right)^2 \right] t^{[\xi]} + \dots, \end{aligned} \quad (2)$$

where  $\phi$  and  $d_i = \varepsilon_i^d d$  represent the  $\alpha$  and deuteron fields with masses  $m_\alpha = 3727.38$  MeV and  $m_d = 1875.61$  MeV, respectively. The coupling constants  $\Delta^{[\xi]}$ ,  $g^{[\xi]}$  and  $h^{[\xi]}$  for each channel cannot be measured directly, but their renormalized values are determined by matching to the available experimental data of phase shifts as we did in the previous work [30]. The dimeron field  $t^{[\xi]}$  with a mass of  $m_t = m_d + m_\alpha$ , and projection operator  $\Pi^{[\xi]}$  for each channel

$\xi$  are defined as

$$t^{[\xi]} = \left\{ \begin{array}{ll} \bar{t}_i, & \xi = {}^3S_1 \\ t, & \xi = {}^3P_0 \\ t_k, & \xi = {}^3P_1 \\ t_{ij}, & \xi = {}^3P_2 \\ \tilde{t}_j, & \xi = {}^3D_1 \\ \tilde{t}_{kl}, & \xi = {}^3D_2 \\ \tilde{t}_{kji}, & \xi = {}^3D_3 \end{array} \right\}, \quad \Pi^{[\xi]} = \left\{ \begin{array}{ll} \varepsilon_i^d, & \xi = {}^3S_1 \\ \sqrt{3} \mathcal{P}_i \varepsilon_i^d, & \xi = {}^3P_0 \\ \sqrt{3/2} \epsilon_{kji} \mathcal{P}_j \varepsilon_i^d, & \xi = {}^3P_1 \\ 3/\sqrt{5} \mathcal{P}_j \varepsilon_i^d, & \xi = {}^3P_2 \\ 3/\sqrt{2} \tau_{ji} \varepsilon_i^d, & \xi = {}^3D_1 \\ \sqrt{3/2} \epsilon_{ijl} \tau_{kj} \varepsilon_i^d, & \xi = {}^3D_2 \\ \sqrt{45/8} \tau_{kj} \varepsilon_i^d, & \xi = {}^3D_3 \end{array} \right\}, \quad (3)$$

with the derivative operators which are introduced as

$$\mathcal{P}_i = \frac{\mu}{i} \left( \frac{\vec{\nabla}_i}{m_d} - \frac{\overleftarrow{\nabla}_i}{m_\alpha} \right), \quad \tau_{ij} = \mathcal{P}_i \mathcal{P}_j - \frac{1}{3} \delta_{ij} \mathcal{P}_k \mathcal{P}_k. \quad (4)$$

The one-body currents are considered by coupling the external photon through minimal substitution,  $\nabla \rightarrow \nabla + ieZ\mathbf{A}$  in the Lagrangian  $\mathcal{L}_{ES}^{[\xi]}$ , where  $Z$  is the charge number and  $\mathbf{A}$  is the photon field. The  $E1$  two-body currents using the auxiliary fields and corresponding projection operators of Eq. 3 for incoming  ${}^3P_0$ ,  ${}^3P_1$  and  ${}^3P_2$  channels can be described as [31]

$$\mathcal{L}_{RC}^{[{}^3P_0]} = -\sqrt{3} \mu Q_1 L_{E1} g^{[{}^3P_0]} g^{[{}^3S_1]} t \bar{t}_i \partial_0 A_i, \quad (5)$$

$$\mathcal{L}_{RC}^{[{}^3P_1]} = -\sqrt{3/2} \mu Q_1 L_{E1} g^{[{}^3P_1]} g^{[{}^3S_1]} \epsilon_{kij} t_k \bar{t}_i \partial_0 A_j, \quad (6)$$

$$\mathcal{L}_{RC}^{[{}^3P_2]} = -3/\sqrt{5} \mu Q_1 L_{E1} g^{[{}^3P_2]} g^{[{}^3S_1]} t_{ij} \bar{t}_i \partial_0 A_j, \quad (7)$$

where  $\mu$  is the reduced mass of the  $d - \alpha$  system. Moreover, the  $E2$  two-body currents for incoming  ${}^3D_1$ ,  ${}^3D_2$  and  ${}^3D_3$  channels are included by the following Lagrangian [32]

$$\mathcal{L}_{RC}^{[{}^3D_1]} = 3/\sqrt{2} \mu Q_2 L_{E2} g^{[{}^3D_1]} g^{[{}^3S_1]} \tilde{t}_j \bar{t}_i \left( \nabla_j \nabla_i A_0 - \partial_0 (\nabla_j A_i + \nabla_i A_j) / 2 \right), \quad (8)$$

$$\mathcal{L}_{RC}^{[{}^3D_2]} = \sqrt{3/2} \mu Q_2 L_{E2} g^{[{}^3D_2]} g^{[{}^3S_1]} \epsilon_{ijl} \tilde{t}_{kl} \bar{t}_i \left( \nabla_k \nabla_j A_0 - \partial_0 (\nabla_k A_j + \nabla_j A_k) / 2 \right), \quad (9)$$

$$\mathcal{L}_{RC}^{[{}^3D_3]} = \sqrt{45/8} \mu Q_2 L_{E2} g^{[{}^3D_3]} g^{[{}^3S_1]} \tilde{t}_{kji} \bar{t}_i \left( \nabla_k \nabla_j A_0 - \partial_0 (\nabla_k A_j + \nabla_j A_k) / 2 \right). \quad (10)$$

The effective charges  $Q_1 = e\mu(Z_d/m_d - Z_\alpha/m_\alpha)$ ,  $Q_2 = e\mu^2(Z_\alpha/m_\alpha^2 + Z_d/m_d^2)$ , and  $g^{[{}^3S_1]}$ ,  $g^{[\xi]}$  factors are included in the definition of the couplings  $L_{E1}$  and  $L_{E2}$ . Here,  $Z_\alpha = 2$  and  $Z_d = 1$  represent the atomic numbers of the alpha particle and deuteron, respectively.

## B. Coulomb interaction

The strength of the Coulomb-photon exchanges in the  $d - \alpha$  interaction is quantified by the dimensionless Sommerfeld parameter  $\eta_p = k_C/p = Z_\alpha Z_d \alpha_{em} \mu/p$ , where  $k_C$  is the

inverse of the Bohr radius of the  $d - \alpha$  system,  $\alpha_{em} = e^2/4\pi \sim 1/137$  represents the fine structure constant and  $p$  is the relative momentum of the alpha and deuteron in the center-of-mass (CM) framework. Since, each photon-exchange insertion is proportional to  $\eta_p$  thus, in the low-energy region where the momentum  $p$  is much less than the characteristic momentum scale  $k_C$ , it is important to take into account the full Coulomb interaction in a non-perturbative manner as illustrated in Fig. 1.

In order to take into account the contribution of the Coulomb interaction in the  $d - \alpha$  system, the Coulomb Green's function is utilized in the following manner [33]. As depicted in Fig. 1, through the integral equation  $\hat{G}_C^\pm = \hat{G}_0^\pm + \hat{G}_0^\pm \hat{V}_C \hat{G}_C^\pm$ , the Coulomb Green's function can be connected to the free Green's function where  $\hat{G}_0^\pm = 1/(E - \hat{H}_0 \pm i\epsilon)$  and  $\hat{G}_C^\pm = 1/(E - \hat{H}_0 - \hat{V}_C \pm i\epsilon)$  are the free and Coulomb Green's functions with  $\hat{V}_C = 2\alpha_{em}/r$  and  $\hat{H}_0 = \hat{p}^2/2\mu$  as the repulsive Coulomb potential between deuteron and alpha and the free Hamiltonian, respectively. The Coulomb wave functions and the retarded Green's function can be obtained by solving the Schrodinger equation with the full Hamiltonian  $\hat{H} = \hat{H}_0 + \hat{V}_C$  as [34, 35]

$$\chi_p^{(+)}(\mathbf{r}) = \sum_{l=0}^{\infty} (2l+1) P_l(\hat{\mathbf{p}} \cdot \hat{\mathbf{r}}) \chi_p^{(l)}(r), \quad (11)$$

$$\chi_p^{(l)}(r) = i^l e^{i\sigma_l} \frac{F_l(\eta_p, pr)}{pr}, \quad (12)$$

$$G_C^{(+)}(E, \mathbf{r}', \mathbf{r}) = \sum_{l=0}^{\infty} (2l+1) P_l(\hat{\mathbf{r}}' \cdot \hat{\mathbf{r}}) G_C^{(l)}(E, r', r), \quad (13)$$

$$G_C^{(l)}(E, r', r) = -\frac{\mu p}{2\pi} \frac{F_l(\eta_p, pr_{<})}{pr_{<}} \frac{H_l^{(+)}(\eta_p, pr_{>})}{pr_{>}}, \quad (14)$$

where  $\sigma_l = \sqrt{\Gamma(l+1+i\eta_p)/\Gamma(l+1-i\eta_p)}$  indicates the pure Coulomb phase shift and  $P_l$  denotes the Legendre function.  $r_{<}$  ( $r_{>}$ ) corresponds to the lesser (greater) of the coordinates  $r, r'$  and

$$F_l(\eta_p, \rho) = C_l(\eta_p) 2^{-l-1} (-i)^{l+1} M_{i\eta_p, l+1/2}(2i\rho), \quad (15)$$

$$H_l^{(+)}(\eta_p, \rho) = (-i)^l e^{\pi\eta_p/2} e^{i\sigma_l} W_{-i\eta_p, l+1/2}(-2i\rho), \quad (16)$$

with conventionally defined the Whittaker functions  $M_{k,\mu}(z)$  and  $W_{k,\mu}(z)$ . The normalized constant  $C_l(\eta_p)$  has the form

$$C_l^2(\eta_p) = \frac{2^{2l} C_0^2(\eta_p) \prod_{n=1}^l (n^2 + \eta_p^2)}{\Gamma(2l+2)^2} = 2^l e^{-\pi\eta_p/2} \frac{|\Gamma(l+1+i\eta_p)|}{\Gamma(2l+2)}, \quad (17)$$

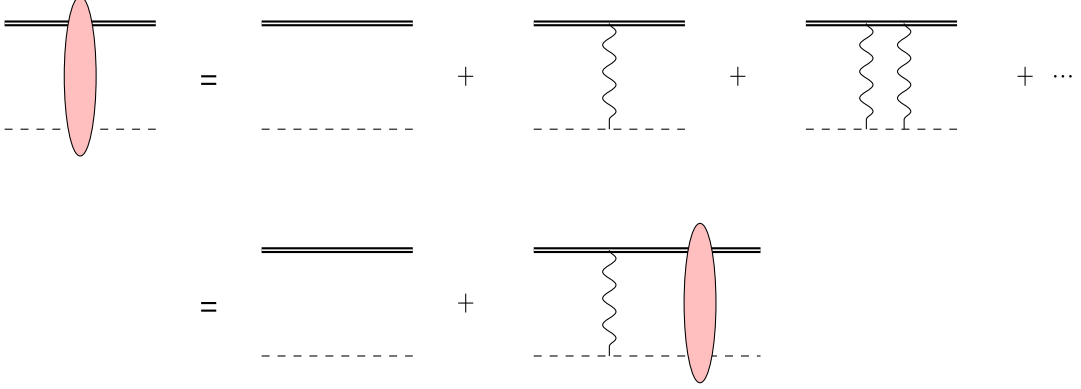


FIG. 1: Coulomb ladder diagrams which illustrate the interaction between scalar alpha and vector deuteron fields. The dashed, double and wavy lines represent the scalar alpha, the vector deuteron field and the exchanged photons, respectively.

where  $C_0^2(\eta_p)$ , is defined as

$$C_0^2(\eta_p) = \chi_{p'}^{(\pm)}(\mathbf{0})\chi_p^{*(\pm)}(\mathbf{0}) = \frac{2\pi\eta_p}{e^{2\pi\eta_p} - 1}. \quad (18)$$

The Coulomb Green's function for  ${}^6\text{Li}$  bound state with two-body binding energy  $B$  is defined as

$$G_C^{(l)}(-B, r', r) = -\frac{i\mu\gamma}{2\pi} \frac{F_l(\eta_{i\gamma}, i\gamma r')}{i\gamma r'} \frac{H_l^{(+)}(\eta_{i\gamma}, i\gamma r)}{i\gamma r}, \quad (19)$$

where  $\gamma = \sqrt{2\mu B}$  indicates the two-body binding momentum of  ${}^6\text{Li}$  and the coordinate space definitions are as  $r' < r$ .

### III. ELASTIC SCATTERING

The elastic scattering amplitude for two charged particles interacting through the long-range Coulomb and short-range strong interactions can be written as [36]

$$T(\mathbf{p}', \mathbf{p}; E) = T_C(\mathbf{p}', \mathbf{p}; E) + T_{CS}(\mathbf{p}', \mathbf{p}; E), \quad (20)$$

where  $\mathbf{p}$  and  $\mathbf{p}'$  denote the relative momentum of incoming and outgoing particles, respectively and  $E = p^2/2\mu$  is the CM energy of the system. These amplitudes are expressed in the partial wave decomposition as [34]

$$T_C(\mathbf{p}', \mathbf{p}; E) = \sum_{l=0}^{\infty} (2l+1) T_C^{[l]} P_l(\hat{\mathbf{p}}' \cdot \hat{\mathbf{p}}) = -\frac{2\pi}{\mu} \sum_{l=0}^{\infty} (2l+1) \frac{e^{2i\sigma_l} - 1}{2ip} P_l(\hat{\mathbf{p}}' \cdot \hat{\mathbf{p}}), \quad (21)$$

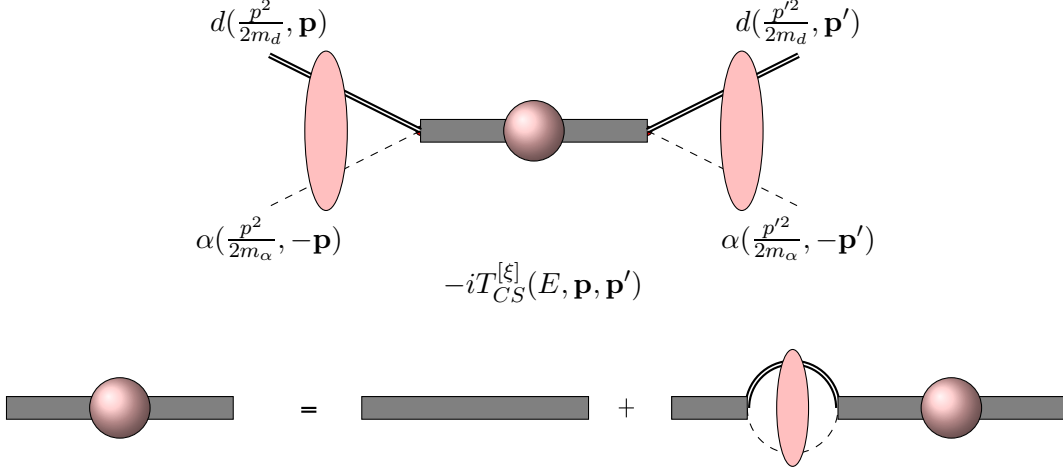


FIG. 2: The elastic scattering amplitude of the  $d - \alpha$  system. The thick line represents the bare dimeron propagator and the thick dashed line with a filled circle is the full dimeron propagator. All remained notations are the same as Fig. 1.

and

$$T_{CS}(\mathbf{p}', \mathbf{p}; E) = \sum_{l=0}^{\infty} (2l+1) T_{CS}^{[l]}(p) e^{2i\sigma_l} P_l(\hat{\mathbf{p}}' \cdot \hat{\mathbf{p}}), \quad (22)$$

with

$$T_{CS}^{[l]}(p) = -\frac{2\pi}{\mu} \frac{1}{p(\cot\delta_l - i)}, \quad (23)$$

where  $\delta_l$  is the Coulomb-corrected phase shift.

For the  $d - \alpha$  elastic scattering, the  $S$ -,  $P$ - and  $D$ -waves ( $\xi = {}^3S_1, {}^3P_0, {}^3P_1, {}^3P_2, {}^3D_1, {}^3D_2, {}^3D_3$ ) dominantly contribute in the cross section at the low-energy region. The CEFT diagram corresponding to the  $d - \alpha$  elastic scattering amplitude is shown in Fig. 2. According to this diagram, the on-shell Coulomb-subtracted EFT amplitudes for each channel  $\xi$  can be obtained as [30]

$$-i(2l+1)T_{CS}^{[\xi]}(p) = -ig^{[\xi]^2} D^{[\xi]}(E, \mathbf{0}) C_0^2(\eta_p) W_l(\eta_p), \quad (24)$$

with the full dimer propagator for channel  $\xi$  as

$$D^{[\xi]}(E, \mathbf{0}) = \frac{\eta^{[\xi]}}{E - \Delta^{[\xi]} + h^{[\xi]} E^2 - \frac{1}{2l+1} \eta^{[\xi]} g^{[\xi]^2} J_l(E)}. \quad (25)$$

On the other hand, the on-shell Coulomb-subtracted amplitude  $T_{CS}^{[\xi]}$  can usually be expressed



in terms of a modified effective range expansion (ERE) as [37]

$$T_{CS}^{[\xi]}(p) = -\frac{2\pi}{\mu} \frac{C_0^2(\eta_p) W_l(\eta_p)}{K^{[\xi]}(p) - H_l(\eta_p)}, \quad (26)$$

with

$$W_l(\eta_p) = \frac{k_C^{2l}}{(l!)^2} \prod_{n=0}^l \left(1 + \frac{n^2}{\eta_p^2}\right), \quad (27)$$

$$H_l(\eta_p) = 2k_C W_l(\eta_p) H(\eta_p), \quad (28)$$

$$H(\eta_p) = \psi(i\eta_p) + \frac{1}{2i\eta_p} - \ln(i\eta_p), \quad (29)$$

where  $\psi$  is the logarithmic derivative of Gamma function.  $K^{[\xi]}(p)$  represents the short-range strong interaction which is obtained in terms of the effective range parameters as [38]

$$K^{[\xi]}(p) = -\frac{1}{a^{[\xi]}} + \frac{1}{2}r^{[\xi]}p^2 + \frac{1}{4}s^{[\xi]}p^4 + \dots, \quad (30)$$

with  $a^{[\xi]}$ ,  $r^{[\xi]}$ , and  $s^{[\xi]}$  as the scattering length, effective range and shape parameter, respectively.

The fully dressed bubble  $J_l$  of Eq. 25, is divergent and requires regularization. We can do this by dividing  $J_l$  into finite and infinite parts as  $J_l = J_l^{fin} + J_l^{div}$ . The finite part is obtained as [39, 40]

$$J_l^{fin}(p) = -\frac{\mu}{2\pi} H_l(\eta_p). \quad (31)$$

The divergent parts absorb in  $g^{[\xi]}$ ,  $\Delta^{[\xi]}$  and  $h^{[\xi]}$ , parameters via introducing the renormalized parameters  $g_R^{[\xi]}$ ,  $\Delta_R^{[\xi]}$  and  $h_R^{[\xi]}$ . The details of these regularizations and renormalizations for all channels are presented in our previous paper [30]. Thus, comparing Eq. 24 to Eq. 26 yields

$$\Delta_R^{[\xi]} = -\frac{\mu\eta^{[\xi]}g_R^{[\xi]^2}}{(2l+1)2\pi a^{[\xi]}}, \quad g_R^{[\xi]^2} = -\frac{(2l+1)2\pi}{\mu^2\eta^{[\xi]}r^{[\xi]}}, \quad h_R^{[\xi]} = -\frac{\mu^3g_R^{[\xi]^2}s^{[\xi]}}{(2l+1)2\pi}. \quad (32)$$

At the binding energy of the ground state of  ${}^6\text{Li}$ , the amplitude should have a pole at the binding momentum  $i\gamma$ . Thus, we have

$$-\frac{1}{a^{[3S_1]}} - \frac{1}{2}r^{[3S_1]}\gamma^2 + \frac{1}{4}s^{[3S_1]}\gamma^4 + \dots - H_0(i\gamma) = 0. \quad (33)$$

By imposing this condition the effective range parameter  $a^{[3S_1]}$  is related to other effective range parameters which can be fixed by available experimental phase shift data of the elastic

$d - \alpha$  scattering. The renormalization constant of the  ${}^6\text{Li}$  wave function which treats as a bound state of alpha and deuteron clusters is defined by the dressed  $S$ -wave dimer propagator as

$$\begin{aligned} \frac{1}{\mathcal{Z}} &= \left. \frac{\partial D^{[{}^3S_1]}(E, \mathbf{0})^{-1}}{\partial E} \right|_{E=-B} \\ &= -\frac{g^{[{}^3S_1]^2} \mu^2}{2\pi p} \frac{\partial}{\partial p} \left( \frac{1}{2} r^{[{}^3S_1]}(p^2 + \gamma^2) + \frac{1}{4} s^{[{}^3S_1]}(p^4 - \gamma^4) + \dots - H_0(\eta_p) + H_0(i\gamma) \right) \Big|_{p=i\gamma}. \end{aligned} \quad (34)$$

#### IV. $E1$ AND $E2$ TRANSITION AMPLITUDES

In this section, we focus on the calculation of the  $E1$  and  $E2$  transition amplitudes for the capture process  $d(\alpha, \gamma){}^6\text{Li}$ . First, the Feynman diagrams of one- and two-body currents that contribute to the dominant transitions ( $E1$  and  $E2$ ) are presented. Then, based on the Feynman rules, the transition amplitudes of diagrams for all possible partial waves  $\xi$ , are presented. As it was mentioned,  $\alpha$  and  $d$  are considered as the point-like nuclei and the  ${}^6\text{Li}$  is the two-body cluster bound state constructed by  $\alpha$  and  $d$ . We assign the initial CM momentum  $\mathbf{p}$  for the  $d - \alpha$  system and the outgoing photon in the final state denoted by  $\mathbf{k}$ .

At the low-energy regime,  $p \leq k_C \sim 18$  MeV, the on-shell CM momentum of the system is scaled as low-momentum  $Q$ . The momentum corresponding to the deuteron binding energy,  $B_d$  i.e.,  $\sqrt{2m_d B_d} \sim 90$  MeV has been considered high-momentum scale  $\Lambda$ . Around the  $p \sim k_C \sim 18$  MeV, the expansion parameter of the current CEFT is estimated of the order  $1/5$ . By increasing the energy, the expansion deteriorates and the precision of our EFT prediction will be questionable for  $E_{CM} = p^2/(2\mu) > 3.3$  MeV.

According to the power counting we count,  $\mu \sim \Lambda^3/Q^2$  and  $\gamma \sim 3Q$ . Thus, the energy-momentum conservation and EFT power counting yield

$$k = \frac{p^2 + \gamma^2}{2\mu} \sim \frac{Q^3}{\Lambda^2} \ll Q \sim p. \quad (35)$$

Thus, in the loop calculation, we can use this approximation

$$E_d + k_0 + q_0 - \frac{(\mathbf{q} + \mathbf{k} + \mathbf{p})^2}{2m_d} \approx E_d + k_0 + q_0 - \frac{(\mathbf{q} + \mathbf{p})^2}{2m_d} \sim \frac{Q^2}{\mu} \sim \frac{Q^4}{\Lambda^3}, \quad (36)$$

with  $E_d = p^2/(2m_d)$ .  $(q_0, \mathbf{q})$  and  $(k_0, \mathbf{k})$  are the loop and photon energy-momentum, respectively. This approximation corresponds to the zero-recoil of the final bound state  ${}^6\text{Li}$ .

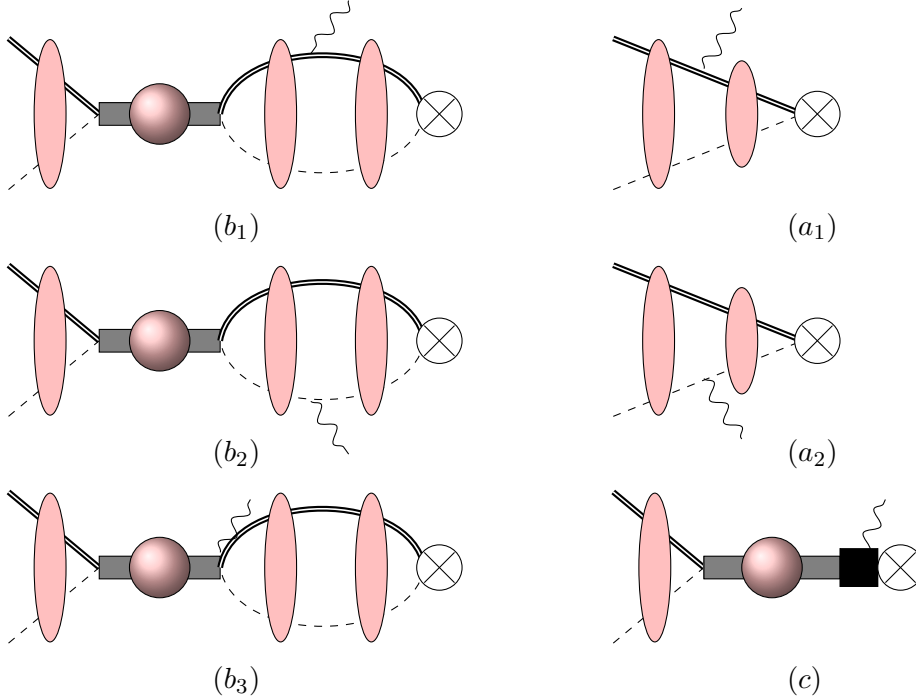


FIG. 3: The diagrams for the radiative capture process  $d(\alpha, \gamma)^6\text{Li}$ . The dashed and double lines represent the scalar alpha and vector deuteron particles respectively. The wavy line indicates the outgoing photon. The square depicts the two-body currents and the  $\otimes$  is the final bound state symbol.

Consequently, we disregard the recoil effect in our calculations up to next-to-next-to-leading order ( $\text{N}^2\text{LO}$ ).

The Feynman diagrams that contribute to the  $d(\alpha, \gamma)^6\text{Li}$  process are shown in Fig. 3. The diagrams  $a_1$  and  $a_2$  are the possible transitions including only Coulomb interactions for the incoming charged particles. The diagrams  $b_1$ ,  $b_2$ , and  $b_3$  involve the initial state short-range interactions. In these diagrams, the external photon minimally couples to one of the single-charged particle lines. The last diagram,  $c$ , denotes the contribution of the two-body current in the gamma capture process. The  $E1$  transition amplitude through all possible incoming  $P$  waves is written as

$$M_{E1}(\mathbf{p}) = \sum_{\xi=^3P_0, ^3P_1, ^3P_2} \left( M_{E1, a_{1,2}}^{[\xi]}(\mathbf{p}) + M_{E1, b_{1,2}}^{[\xi]}(\mathbf{p}) + M_{E1, b_3}^{[\xi]}(\mathbf{p}) + M_{E1, c}^{[\xi]}(\mathbf{p}) \right). \quad (37)$$

As shown in the following, this amplitude leads to

$$M_{E1}(\mathbf{p}) = \mathcal{M}_{E1}(p) \varepsilon_i^d \varepsilon_j^{Li*} (\boldsymbol{\varepsilon}^{\gamma*} \cdot \hat{\mathbf{p}}), \quad (38)$$

where  $\boldsymbol{\varepsilon}^\gamma$  denotes the polarization vector of the outgoing photon and  $\boldsymbol{\varepsilon}^d$  and  $\boldsymbol{\varepsilon}^{Li}$  are spin polarization vectors of  $d$  and  ${}^6\text{Li}$ , respectively. The  $E1$  transition amplitudes from the initial  ${}^3P_0$ ,  ${}^3P_1$ , and  ${}^3P_2$  states to the final bound state  ${}^3S_1$ , corresponding to the diagrams  $a_1$ ,  $a_2$ ,  $b_1$ ,  $b_2$ ,  $b_3$  and  $c$  are obtained as

$$\begin{aligned} M_{E1,a_{1,2}}^{[\xi]}(\mathbf{p}) &= \frac{i}{\mu} Q_1 g^{[{}^3S_1]} \sqrt{\mathcal{Z}} \varepsilon_i^d \varepsilon_j^{Li*} \varepsilon_k^{\gamma*} \int d^3r G_C^{(0)}(-B, 0, r) \nabla_k [{}^3P_1(\hat{\mathbf{p}} \cdot \hat{\mathbf{r}}) \chi_p^{(1)}(r)] \\ &= 2 Q_1 g^{[{}^3S_1]} \sqrt{\mathcal{Z}} C_0(\eta_p) e^{i\sigma_1} \mathcal{A}_1(p) \varepsilon_i^d \varepsilon_j^{Li*} (\boldsymbol{\varepsilon}^{\gamma*} \cdot \hat{\mathbf{p}}), \end{aligned} \quad (39)$$

$$\begin{aligned} M_{E1,b_{1,2}}^{[\xi]}(\mathbf{p}) &= \frac{1}{\mu} Q_1 g^{[{}^3S_1]} \sqrt{\mathcal{Z}} \varepsilon_i^d \varepsilon_j^{Li*} \varepsilon_k^{\gamma*} \frac{3T_{CS}^{[\xi]}(p) e^{i\sigma_1}}{C_0(\eta_p) W_1^{1/2}(\eta_p)} \hat{\mathbf{p}}_l \\ &\quad \times \int d^3r G_C^{(0)}(-B, 0, r) \lim_{r'' \rightarrow 0} \nabla_k \nabla_l'' [{}^3P_1(\hat{\mathbf{r}} \cdot \hat{\mathbf{r}}'') G_C^{(1)}(E, r, r'')] \\ &= 2 Q_1 g^{[{}^3S_1]} \sqrt{\mathcal{Z}} \frac{C_0(\eta_p) W_1^{1/2}(\eta_p)}{K^{[\xi]}(p) - H_1(\eta_p)} e^{i\sigma_1} \mathcal{B}_1(p) \varepsilon_i^d \varepsilon_j^{Li*} (\boldsymbol{\varepsilon}^{\gamma*} \cdot \hat{\mathbf{p}}), \end{aligned} \quad (40)$$

$$\begin{aligned} M_{E1,b_3}^{[\xi]}(\mathbf{p}) &= i Q_1 g^{[{}^3S_1]} \sqrt{\mathcal{Z}} \varepsilon_i^d \varepsilon_j^{Li*} \varepsilon_k^{\gamma*} G_C^{(0)}(-B, 0, 0) \frac{3T_{CS}^{[\xi]}(p) e^{i\sigma_1}}{C_0(\eta_p) W_1^{1/2}(\eta_p)} \hat{\mathbf{p}}_k \\ &= -\frac{6\pi i}{\mu} Q_1 g^{[{}^3S_1]} \sqrt{\mathcal{Z}} \frac{C_0(\eta_p) W_1^{1/2}(\eta_p)}{K^{[\xi]}(p) - H_1(\eta_p)} e^{i\sigma_1} J_0(i\gamma) \varepsilon_i^d \varepsilon_j^{Li*} (\boldsymbol{\varepsilon}^{\gamma*} \cdot \hat{\mathbf{p}}), \end{aligned} \quad (41)$$

$$\begin{aligned} M_{E1,c}^{[\xi]}(\mathbf{p}) &= i\mu k_0 Q_1 g^{[{}^3S_1]} \sqrt{\mathcal{Z}} \varepsilon_i^d \varepsilon_j^{Li*} \varepsilon_k^{\gamma*} L_{E1} \frac{3T_{CS}^{[\xi]}(p) e^{i\sigma_1}}{C_0(\eta_p) W_1^{1/2}(\eta_p)} \hat{\mathbf{p}}_k \\ &= -6i\pi k_0 L_{E1} Q_1 g^{[{}^3S_1]} \sqrt{\mathcal{Z}} \frac{C_0(\eta_p) W_1^{1/2}(\eta_p)}{K^{[\xi]}(p) - H_1(\eta_p)} e^{i\sigma_1} \varepsilon_i^d \varepsilon_j^{Li*} (\boldsymbol{\varepsilon}^{\gamma*} \cdot \hat{\mathbf{p}}). \end{aligned} \quad (42)$$

with

$$\mathcal{A}_1(p) = \frac{\Gamma(1+k_C/\gamma)}{C_0(\eta_p)} \int_0^\infty dr r W_{-k_C/\gamma, 1/2}(2\gamma r) \left(3 + r \frac{\partial}{\partial r}\right) \frac{F_1(\eta_p, pr)}{pr^2}, \quad (43)$$

$$\mathcal{B}_1(p) = ip \Gamma(1+k_C/\gamma) \Gamma(2+i\eta_p) \int_0^\infty dr r W_{-k_C/\gamma, 1/2}(2\gamma r) \left(\frac{2}{r} + \frac{\partial}{\partial r}\right) \frac{W_{-i\eta_p, 3/2}(-2ipr)}{r}. \quad (44)$$

We are working in Coulomb gauge where the relation  $\boldsymbol{\varepsilon}^\gamma \cdot \mathbf{k} = 0$  for the real photon with momentum  $\mathbf{k}$  is fulfilled. Also, the spherical symmetry  $r_i r_j / r^2 \rightarrow \delta_{ij} / 3$  is used in the integrals of Eqs. 39 and 40. The Whittaker function  $W_{-k_C/\gamma, 1/2}(2\gamma r)$ , in diagrams  $a_1$ ,  $a_2$ ,  $b_1$  and  $b_2$  is associated with the final  $S$ -wave bound state wave function and the  $P$ -wave Coulomb wave function  $F_1(\eta_p, pr)$  in  $a_1$  and  $a_2$  diagrams corresponds to the initial incoming scattering

state [41]. Moreover, due to the presence of one bound-state field, there is a wave function renormalization  $\sqrt{\mathcal{Z}}$  present. Thus, the  $E1$  transition amplitude for the  $d(\alpha, \gamma)^6\text{Li}$  process is summarized as

$$\mathcal{M}_{E1}(p) = 2 Q_1 g^{[3S_1]} \sqrt{\mathcal{Z}} C_0(\eta_p) e^{i\sigma_1} \left[ \mathcal{A}_1(p) + \frac{W_1^{1/2}(\eta_p)}{K^{[\xi]}(p) - H_1(\eta_p)} \left( \mathcal{B}_1(p) - \frac{3\pi i}{\mu} J_0(i\gamma) - 3\pi i k_0 L_{E1} \right) \right]. \quad (45)$$

Increasing the CM energy, the  $E2$  transition would be more important in the  $d(\alpha, \gamma)^6\text{Li}$  reaction. So, we should consider the contribution of the  $E2$  transition to include  $3^+$  resonance at  $E_{CM} = 0.71$  MeV in the current study. So, in the following, the  $E2$  transition for  $d(\alpha, \gamma)^6\text{Li}$  reaction which involves transition from  ${}^3D_1$ ,  ${}^3D_2$  and  ${}^3D_3$  to  ${}^3S_1$  would be considered. The contribution of all diagrams in the  $E2$  transition can be summarized as

$$M_{E2}(\mathbf{p}) = \sum_{\xi=3D_1, 3D_2, 3D_3} (M_{E2, a_{1,2}}^{[\xi]}(\mathbf{p}) + M_{E2, b_{1,2}}^{[\xi]}(\mathbf{p}) + M_{E2, b_3}^{[\xi]}(\mathbf{p}) + M_{E2, c}^{[\xi]}(\mathbf{p})), \quad (46)$$

with

$$M_{E2}(\mathbf{p}) = \mathcal{M}_{E2}(p) \varepsilon_i^d \varepsilon_j^{Li*} (\hat{\mathbf{k}} \cdot \hat{\mathbf{p}}) (\boldsymbol{\varepsilon}^{\gamma*} \cdot \hat{\mathbf{p}}). \quad (47)$$

The  $E2$  transition amplitude from the initial  ${}^3D_1$ ,  ${}^3D_2$ , and  ${}^3D_3$  states to the final bound state  ${}^3S_1$ , for the diagrams  $a_1$ ,  $a_2$ ,  $b_1$ ,  $b_2$  and  $b_3$  are obtained as

$$\begin{aligned} M_{E2, a_{1,2}}^{[\xi]}(\mathbf{p}) &= -\frac{1}{\mu} Q_2 g^{[3S_1]} \sqrt{\mathcal{Z}} \varepsilon_i^d \varepsilon_j^{Li*} \varepsilon_k^{\gamma*} k_l \int d^3r G_C^{(0)}(-B, 0, r) r_l \nabla_k [5P_2(\hat{\mathbf{p}} \cdot \hat{\mathbf{r}}) \chi_p^{(2)}(r)], \\ &= -2k Q_2 g^{[3S_1]} \sqrt{\mathcal{Z}} e^{i\sigma_2} \mathcal{A}_2(p) \varepsilon_i^d \varepsilon_j^{Li*} (\hat{\mathbf{k}} \cdot \hat{\mathbf{p}}) (\boldsymbol{\varepsilon}^{\gamma*} \cdot \hat{\mathbf{p}}), \end{aligned} \quad (48)$$

$$\begin{aligned} M_{E2, b_{1,2}}^{[\xi]}(\mathbf{p}) &= \frac{i}{\mu} Q_2 g^{[3S_1]} \sqrt{\mathcal{Z}} \varepsilon_i^d \varepsilon_j^{Li*} \varepsilon_k^{\gamma*} \frac{5T_{CS}^{[\xi]}(p) e^{i\sigma_2}}{C_0(\eta_p) W_2^{1/2}(\eta_p)} (\hat{\mathbf{p}}_n \hat{\mathbf{p}}_m - \frac{1}{3} \delta_{nm}) k_l \int d^3r \\ &\quad \times G_C^{(0)}(-B, 0, r) r_l \nabla_k \lim_{\mathbf{r}'' \rightarrow 0} (\nabla_n'' \nabla_m'' - \frac{1}{3} \delta_{nm} \nabla_n'' \nabla_m'') [5P_2(\hat{\mathbf{r}} \cdot \hat{\mathbf{r}}'') G_C^{(2)}(E, r, r'')] \\ &= -\frac{2i}{3} k Q_2 g^{[3S_1]} \sqrt{\mathcal{Z}} \frac{C_0(\eta_p) W_2^{1/2}(\eta_p)}{K^{[\xi]}(p) - H_2(\eta_p)} e^{i\sigma_2} \mathcal{B}_2(p) \varepsilon_i^d \varepsilon_j^{Li*} (\hat{\mathbf{k}} \cdot \hat{\mathbf{p}}) (\boldsymbol{\varepsilon}^{\gamma*} \cdot \hat{\mathbf{p}}), \end{aligned} \quad (49)$$

$$\begin{aligned} M_{E2, b_3}^{[\xi]}(\mathbf{p}) &= -Q_2 g^{[3S_1]} \sqrt{\mathcal{Z}} \varepsilon_i^d \varepsilon_j^{Li*} \varepsilon_k^{\gamma*} k_l G_C^{(0)}(-B, 0, 0) \frac{5T_{CS}^{[\xi]}(p) e^{i\sigma_2}}{C_0(\eta_p) W_2^{1/2}(\eta_p)} (\hat{\mathbf{p}}_k \hat{\mathbf{p}}_l - \frac{1}{3} \delta_{kl}) \\ &= \frac{10\pi}{\mu} k Q_2 g^{[3S_1]} \sqrt{\mathcal{Z}} \frac{C_0(\eta_p) W_2^{1/2}(\eta_p)}{K^{[\xi]}(p) - H_2(\eta_p)} e^{i\sigma_2} J_0(i\gamma) \varepsilon_i^d \varepsilon_j^{Li*} (\hat{\mathbf{k}} \cdot \hat{\mathbf{p}}) (\boldsymbol{\varepsilon}^{\gamma*} \cdot \hat{\mathbf{p}}), \end{aligned} \quad (50)$$

$$\begin{aligned}
M_{E2,c}^{[\xi]}(\mathbf{p}) &= -\mu Q_2 g^{[3S_1]} \sqrt{\mathcal{Z}} \varepsilon_i^d \varepsilon_j^{Li*} L_{E1} k_0 \varepsilon_k^{\gamma*} k_l \frac{5T_{CS}^{[\xi]}(p) e^{i\sigma_2}}{C_0(\eta_p) W_2^{1/2}(\eta_p)} (\hat{\mathbf{p}}_k \hat{\mathbf{p}}_l - \frac{1}{3} \delta_{kl}) \\
&= 10\pi k k_0 Q_2 g^{[3S_1]} \sqrt{\mathcal{Z}} L_{E2} \frac{C_0(\eta_p) W_2^{1/2}(\eta_p)}{K^{[\xi]}(p) - H_2(\eta_p)} e^{i\sigma_2} \varepsilon_i^d \varepsilon_j^{Li*} (\hat{\mathbf{k}} \cdot \hat{\mathbf{p}}) (\boldsymbol{\varepsilon}^{\gamma*} \cdot \hat{\mathbf{p}}), \quad (51)
\end{aligned}$$

with

$$\mathcal{A}_2(p) = \frac{\Gamma(1 + \frac{k_C}{\gamma})}{C_0(\eta_p)} \int_0^\infty dr r^2 W_{-k_C/\gamma, 1/2}(2\gamma r) \left( \frac{3}{r} + \frac{\partial}{\partial r} \right) \frac{F_2(\eta_p, pr)}{pr}, \quad (52)$$

$$\mathcal{B}_2(p) = -p^2 \Gamma(1 + \frac{k_C}{\gamma}) \Gamma(3 + i\eta_p) \int_0^\infty dr r^2 W_{-k_C/\gamma, 1/2}(2\gamma r) \left( \frac{3}{r} + \frac{\partial}{\partial r} \right) \frac{W_{-i\eta_p, 5/2}(-2ipr)}{r}. \quad (53)$$

The spherical symmetry is used to write  $r_k r_j r_i r_l / r^4 \rightarrow (\delta_{kj} \delta_{il} + \delta_{ki} \delta_{jl} + \delta_{kl} \delta_{ji}) / 15$  in the integrals. Thus, the  $E2$  transition amplitude for the  $d(\alpha, \gamma)^6\text{Li}$  capture reaction from the initial  $D$ -wave states is summarized as

$$\begin{aligned}
\mathcal{M}_{E2}^{[\xi]}(p) &= -2k Q_2 g^{[3S_1]} \sqrt{\mathcal{Z}} C_0(\eta_p) e^{i\sigma_2} \\
&\times \left[ \mathcal{A}_2(p) + \frac{W_2^{1/2}(\eta_p)}{K^{[\xi]}(p) - H_2(\eta_p)} \left( \frac{i}{3} \mathcal{B}_2(p) - \frac{5\pi}{\mu} J_0(i\gamma) - 5\pi k_0 L_{E2} \right) \right]. \quad (54)
\end{aligned}$$

The loops of the diagrams  $b_1$  and  $b_2$  lead to a logarithmic divergence in  $M_{E1, b_{1,2}}^{[\xi]}$  and  $M_{E2, b_{1,2}}^{[\xi]}$  amplitudes when  $r$  goes to zero. A short range cutoff  $r_C$  in the  $r$  integral in Eqs. 44 and 53 is introduced as a regulator and the divergence can be handled by renormalizing the counter terms  $L_{E1}$  and  $L_{E2}$  [42], [43]. The loop of the diagram  $b_3$  is also divergent and could be renormalized by the  $L_{E1}$  and  $L_{E2}$  terms as well. By extracting the divergent parts, the renormalized  $L_{E1}$  and  $L_{E2}$  can be expressed as

$$L_{E1}^R = L_{E1} + \frac{1}{\mu k_0} \left[ J_0^{div} + \frac{i\mu}{3\pi} \mathcal{B}_1^{div} \right], \quad (55)$$

$$L_{E2}^R = L_{E2} + \frac{1}{\mu k_0} \left[ J_0^{div} - \frac{i\mu}{15\pi} \mathcal{B}_2^{div} \right], \quad (56)$$

with

$$\mathcal{B}_1^{div} = \mathcal{B}_2^{div} = k_C \int_0^{r_C} \frac{dr}{r} \rightarrow k_C \left( \frac{\kappa}{2} \right)^{2\epsilon} \int_0^{r_C} \frac{dr}{r^{1-2\epsilon}} = k_C \left[ \frac{1}{2\epsilon} + \ln\left(\frac{\kappa}{2} r_C\right) + \mathcal{O}(\epsilon) \right]. \quad (57)$$

In the power divergence subtraction (PDS) regularization scheme, the divergent part of  $J_0$  that does not depend on the momentum is obtained as [44]

$$J_0^{div} = \frac{\mu k_C}{2\pi} \left[ \frac{1}{\epsilon} + \ln\left(\frac{\pi \kappa^2}{4k_C^2}\right) + 2 - 3C_E \right], \quad (58)$$

with  $D$  the dimensionality of spacetime,  $\kappa$  the renormalization mass scale and  $C_E = 0.577\dots$  Euler–Mascheroni constant. The  $L_{E1}^R$  and  $L_{E2}^R$  refer to the renormalized parameters that have been adjusted with fitting to the astrophysical S-factor experimental data.

## V. RESULTS

The astrophysical S-factor plays a crucial role in the nuclear fusion reactions in the core of stars. This factor allows us to calculate how quickly those reactions take place and take into account the interaction between the reacting particles. It defines as

$$S(E) \equiv E \exp(2\pi\eta_p) \sigma(p), \quad (59)$$

where  $\sigma(p)$  denotes the total cross-section. The differential cross section for our reaction is calculated by averaging over the initial spin and summing over all components of the final state i.e., the outgoing photon polarization and the  ${}^6\text{Li}$  spin components as

$$\frac{d\sigma}{d\Omega} = \frac{\mu k}{8\pi^2 p} \frac{1}{9} \sum_{i,j=1}^3 \sum_{r=1}^2 \left| [\mathcal{M}_{E1}(p) + \mathcal{M}_{E2}(p)(\hat{\mathbf{k}} \cdot \hat{\mathbf{p}})] (\boldsymbol{\varepsilon}_r^{\gamma*} \cdot \hat{\mathbf{p}}) \varepsilon_i^d \varepsilon_j^{Li*} \right|^2, \quad (60)$$

by considering photon momentum direction  $\hat{\mathbf{k}}$  along  $\hat{z}$  axis and integrating over angle variables. The total cross section is presented by

$$\sigma(p) = \frac{\mu k}{18\pi p} \left( |\mathcal{M}_{E1}(p)|^2 + \frac{1}{5} |\mathcal{M}_{E2}(p)|^2 \right). \quad (61)$$

To calculate the S-factor using the EFT expressions for the  $E1$  and  $E2$  transition amplitudes of Eqs. 45 and 54, we need to determine the values of the elastic  $P$ - and  $D$ - waves scattering parameters and the  $E1$  and  $E2$  two-body coupling constants. Recently,  $S$ -,  $P$ -, and  $D$ -wave scattering parameters have been obtained by phase shift analysis in our previous paper [30]. For the  $E1$  and  $E2$  two-body coupling constants  $L_{E1}^R$  and  $L_{E2}^R$ , we have matched our EFT relation for the S-factor to the available experimental data [1, 18–22] at the energy range 0.001 – 3.3 MeV with arbitrary values of the cutoff  $r_C$ . Table II shows the results of the S-factor in energies  $E_{CM} = 0.2$  and 3 MeV as a function of  $r_C$ . The  $L_{E1}^R$  and  $L_{E2}^R$  constants and the S-factor demonstrate a notable correlation with the short-range cutoff  $r_C$ . As the radius  $r_C$  decreases, the S-factor increases gradually. It can be seen for the cutoff values below  $r_C = 0.1$  fm, the values of the S-factor would be stable. This indicates the insensitivity of the S-factor to the precisely chosen short-range cutoff within the region of  $r_C \leq 0.1$  fm.

TABLE II: Fitted values of the  $L_{E1}^R$  and  $L_{E2}^R$  constants to experimental data of S-factor at  $E_{CM} = 0.001 - 3.3$  MeV with the cutoff  $r_C = 0.001 - 1$  fm. In the fourth and the last columns, the results of S-factor at  $E_{CM} = 0.2$  MeV and  $E_{CM} = 3$  MeV are presented.

$r_C$ (fm)	$L_{E1}^R$	$L_{E2}^R$	S-factor(MeV.b) ( $E_{CM} = 0.2$ MeV)	S-factor(MeV.b) ( $E_{CM} = 3$ MeV)
1	$(5.805 \pm 0.881) \times 10^{-1}$	$2.197 \pm 0.383$	$4.841 \times 10^{-9}$	$3.271 \times 10^{-7}$
0.5	$(5.421 \pm 0.732) \times 10^{-1}$	$1.945 \pm 0.326$	$4.985 \times 10^{-9}$	$3.724 \times 10^{-7}$
0.2	$(5.187 \pm 0.865) \times 10^{-1}$	$1.621 \pm 0.293$	$5.171 \times 10^{-9}$	$3.993 \times 10^{-7}$
0.1	$(4.942 \pm 0.719) \times 10^{-1}$	$1.352 \pm 0.318$	$5.312 \times 10^{-9}$	$4.083 \times 10^{-7}$
0.05	$(4.733 \pm 0.748) \times 10^{-1}$	$1.349 \pm 0.304$	$5.319 \times 10^{-9}$	$4.101 \times 10^{-7}$
0.001	$(4.721 \pm 0.752) \times 10^{-1}$	$1.344 \pm 0.315$	$5.320 \times 10^{-9}$	$4.103 \times 10^{-7}$

According to the power counting proposed in Sec. IV, the dominant contributions of the scattering amplitude in channels  ${}^3P_0$ ,  ${}^3P_1$ ,  ${}^3P_2$ ,  ${}^3D_1$  and  ${}^3D_2$  come from their scattering lengths and the influences of both their effective ranges and shape parameters are small and can be considered as higher-order corrections [30]. Based on this power counting the effective charges  $Q_1$  and  $Q_2$  scale as  $Q^4/\Lambda^4$  and  $Q/\Lambda$ , respectively. Also we consider  $\mathcal{B}_2/\mathcal{A}_2 \sim \Lambda^4/Q^2$  and  $\mathcal{B}_1/\mathcal{A}_1 \sim Q^2\Lambda$  which hold over a range of  $0.1 \text{ MeV} \lesssim E_{CM} \lesssim 3.3 \text{ MeV}$ . Taking into account these analyses, we can estimate the order of all diagrams in both  $E1$  and  $E2$  transition amplitudes for each channel. In Table III, the relative contribution of diagrams  $b_{1,2}$ ,  $b_3$  and  $c$  for each channel to the diagrams  $a_{1,2}$  in channel  ${}^3D_3$  are presented. It is shown the LO contribution comes from the diagrams  $b_3$  and  $c$  in the  ${}^3D_3$  channel that can independently reproduce the resonance of the S-factor observed at  $E_{CM} = 0.71$  MeV. Around the resonance energy, the  $a_{1,2}$  diagrams for all  $D$ -waves can be considered as NLO corrections. Additionally, the  $b_3$  and  $c$  diagrams corresponding to the  ${}^3D_1$  and  ${}^3D_2$  waves along with the  $a_{1,2}$  diagrams for all  $P$  waves have N<sup>2</sup>LO contribution same as the  $b_{1,2}$ ,  $b_3$  and  $c$  diagrams for the  ${}^3P_0$  channel. The remained diagrams in Table III are affected by S-factor as higher-order corrections.

In Fig. 4, the contributions of each partial wave in our EFT calculation for the astrophysical S-factor of the capture reaction  $d(\alpha, \gamma){}^6\text{Li}$  are presented. It shows that the primary contribution comes from the initial  ${}^3P_2$  partial wave at energies below 0.1 MeV in the CM



TABLE III: The relative contribution of diagrams  $b_{1,2}$ ,  $b_3$ ,  $c$  for each channel to the diagrams  $a_{1,2}$  for channel  ${}^3D_3$  around the resonance energy  $E_{CM} = 0.71$  MeV, according to the suggested power counting.

$\xi$	$\mathcal{M}_{E_1,a_{1,2}}^{[\xi]}/\mathcal{M}_{E_2,a_{1,2}}^{[\xi]}$	$\mathcal{M}_{E_1,b_{1,2}}^{[\xi]}/\mathcal{M}_{E_2,a_{1,2}}^{[\xi]}$	$\mathcal{M}_{E_1,b_3}^{[\xi]}/\mathcal{M}_{E_2,a_{1,2}}^{[\xi]}$	$\mathcal{M}_{E_1,c}^{[\xi]}/\mathcal{M}_{E_2,a_{1,2}}^{[\xi]}$
${}^3P_0$	$Q/\Lambda$	$Q/\Lambda$	$Q/\Lambda$	$Q/\Lambda$
${}^3P_1$	$Q/\Lambda$	$Q^2/\Lambda^2$	$Q^2/\Lambda^2$	$Q^2/\Lambda^2$
${}^3P_2$	$Q/\Lambda$	$Q^2/\Lambda^2$	$Q^2/\Lambda^2$	$Q^2/\Lambda^2$
$\xi$	$\mathcal{M}_{E_2,a_{1,2}}^{[\xi]}/\mathcal{M}_{E_2,a_{1,2}}^{[\xi]}$	$\mathcal{M}_{E_2,b_{1,2}}^{[\xi]}/\mathcal{M}_{E_2,a_{1,2}}^{[\xi]}$	$\mathcal{M}_{E_2,b_3}^{[\xi]}/\mathcal{M}_{E_2,a_{1,2}}^{[\xi]}$	$\mathcal{M}_{E_2,c}^{[\xi]}/\mathcal{M}_{E_2,a_{1,2}}^{[\xi]}$
${}^3D_1$	1	$Q^4/\Lambda^4$	$Q/\Lambda$	$Q/\Lambda$
${}^3D_2$	1	$Q^4/\Lambda^4$	$Q/\Lambda$	$Q/\Lambda$
${}^3D_3$	1	$Q^2/\Lambda^2$	$\Lambda/Q$	$\Lambda/Q$

framework. Moving into the resonance region, the  ${}^3D_3$  channel becomes the dominant contribution which makes the resonance at  $E_{CM} = 0.71$  MeV. The EFT results indicated in Fig. 4 are in agreement with the power counting estimations in Table III. Also, the contributions of  $E1$ ,  $E2$ , and the  $E1 + E2$  transitions of the astrophysical S-factor for the capture reaction  $d(\alpha, \gamma){}^6\text{Li}$  are shown in Fig. 5. The  $E1$  transition from  $P$ -waves to the  ${}^6\text{Li}$  ground state is significantly hindered by the isospin selection rule for  $N = Z$  nuclei due to the nearly identical charge-to-mass ratios of the deuteron and the  $\alpha$  particle. As we expect the  $E1$  capture will be more dominant than the  $E2$  capture at energies lower than 0.1 MeV due to the different energy dependencies of the penetration probabilities in the  $P$ - and  $D$ -waves. In contrast, the  $E2$  component becomes more significant at energies related to resonance energy and higher. Finally, the result obtained for the astrophysical S-factor based on the cluster EFT approach has been compared with the results obtained from two other theoretical approaches in Fig. 6 [9, 11].

## VI. CONCLUSION

In this paper, we have studied the gamma capture reaction  $d(\alpha, \gamma){}^6\text{Li}$ , with the two-body CEFT approach at low energy region. we have concentrated on the energy region  $E_{CM} \lesssim 3.3$  MeV. In this energy region, the Coulomb force was considered non-perturbatively. In

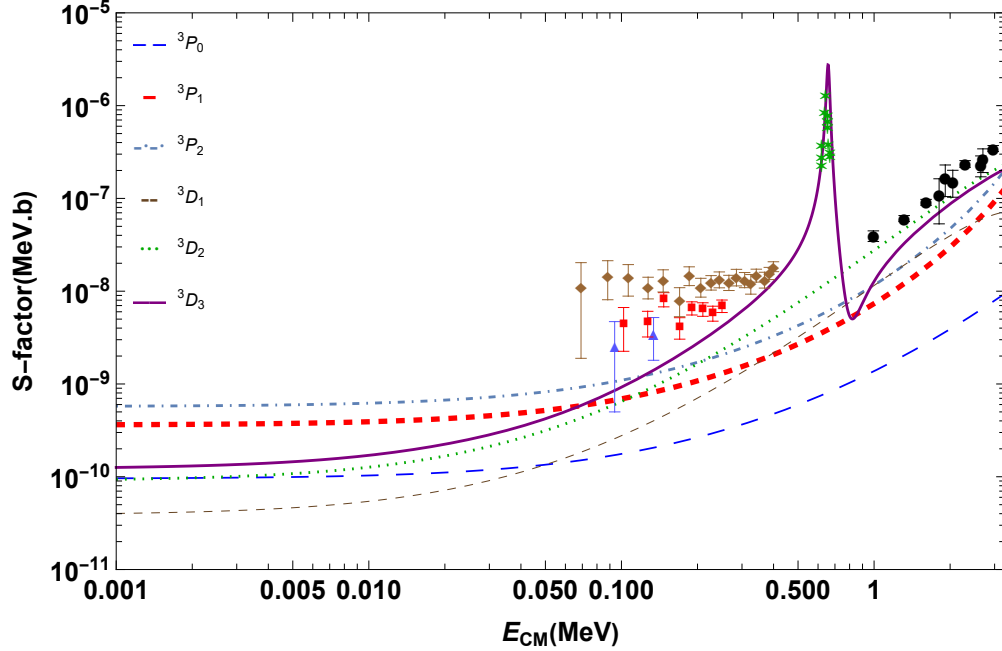


FIG. 4: Contributions of the different incoming partial waves components in our calculated EFT astrophysical S-factor for the capture reaction  $d(\alpha, \gamma)^6\text{Li}$  compared with the experimental data of direct measurements: black circles [18], red triangles[19], green stars [20], brown diamonds [21], blue squares[22].

the study of the radiative capture reaction  $d(\alpha, \gamma)^6\text{Li}$ , we calculate the radiative capture amplitudes for the initial  $P$ - and  $D$ -waves of the  $d - \alpha$  system. The  $E1$  transition from initial  $P$ -wave states to the ground state of  $^6\text{Li}$  was considered and the  $E2$  transition contains  $D$ -wave initial states. Our EFT results in Fig. 4 illustrate the significance of  $l \leq 2$  partial waves in the astrophysical S-factor of  $d(\alpha, \gamma)^6\text{Li}$  reaction.

It is evident that at energies below 0.1 MeV in the CM framework, the primary contribution comes from the initial  $^3P_2$  partial wave. Moving into the resonance region, the  $^3D_3$  channel becomes the dominant contribution, making the resonance at  $E_{CM} = 0.71\text{MeV}$ . Below an energy threshold of 0.1 MeV in the CM frame, the primary influence stems from the initial  $^3P_2$  partial wave.

Next, we analyzed the cluster EFT results for the  $E1$  and  $E2$  contributions, contrasting them with existing experimental data. In Fig. 5, the  $E1$ ,  $E2$ , and combined  $E1+E2$  transitions of the astrophysical S-factor for the  $d(\alpha, \gamma)^6\text{Li}$  reaction are represented. The primary role of the  $E1$  transition is emphasized in the astrophysical S-factor of the gamma

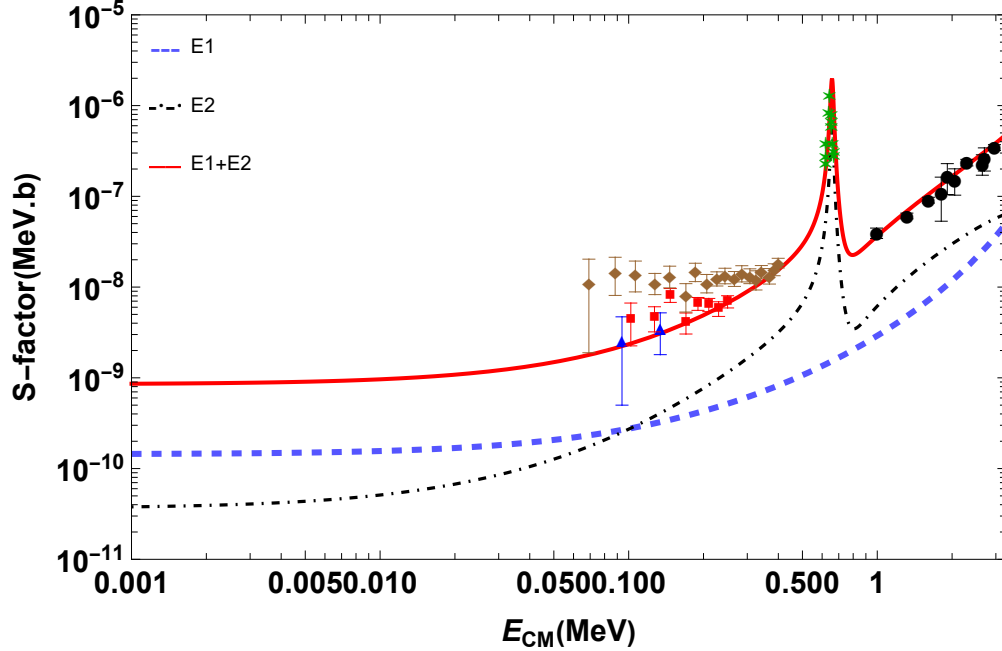


FIG. 5: The contribution of the  $E1$  and  $E2$ , and the  $E1 + E2$  transitions to the astrophysical S-factor for the capture reaction  $d(\alpha, \gamma)^6\text{Li}$  according to our cluster effective field theory approach. In this figure, the order of each diagram is also shown. The experimental data are the same as Fig. 4.

capture reaction  $d(\alpha, \gamma)^6\text{Li}$  for energies below 0.1 MeV. Once the energy surpasses this threshold, the dominance shifts towards the  $E2$  channel. It has been determined that the  $E2$  transition specifically through the two-body current diagram plays a significant role in accurately capturing the resonance behavior observed at energies above 0.1 MeV.

It seems that in the current CEFT calculations which assume the deuteron as a point-like particle, the results for  $E_{CM} > 3.3$  MeV are controversial. Utilizing the three-body cluster formalism is vital for precisely understanding and calculating cross-sections at elevated energies. To resolve the disparities in the S-factor findings for CM energies exceeding 3.3 MeV, a three-body cluster effective field theory method can be utilized. This method views the neutron, proton, and alpha particles as relevant degrees of freedom.

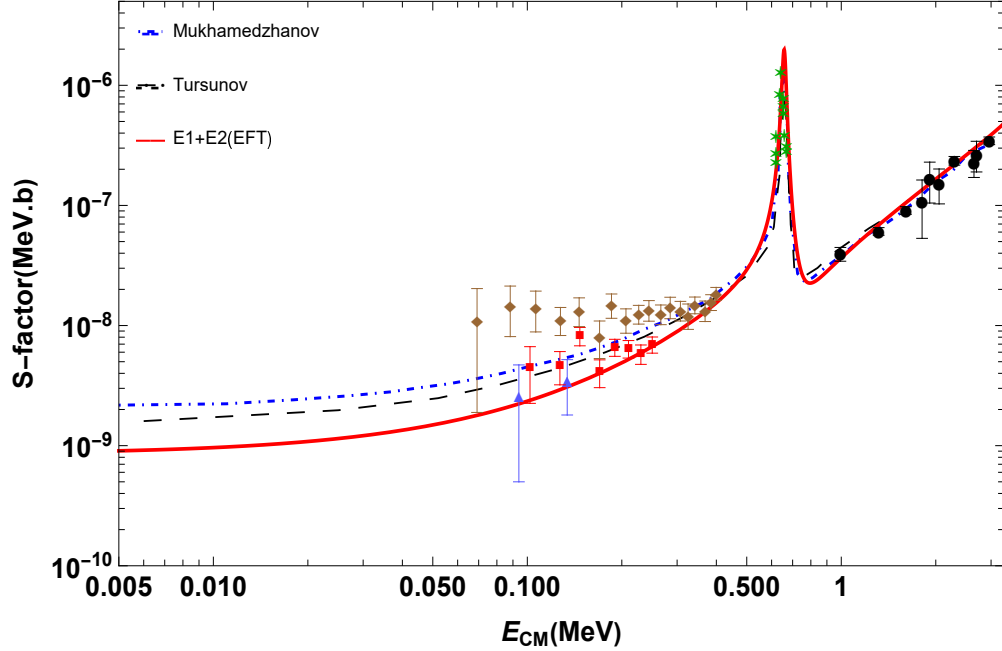


FIG. 6: Comparison of the result obtained for astrophysical S-factor from cluster EFT approach with the results obtained from two other theoretical approaches [9, 11].

### Acknowledgment

This work is based upon research funded by Iran National Science Foundation (INSF) under project No. 4003662. We are grateful to Dr. Ergash Tursunov for sharing the experimental data.

- 
- [1] D Trezzi, M Anders, M Aliotta, A Bellini, D Bemmerer, A Boeltzig, C Brogini, CG Bruno, A Cacioli, F Cavanna, et al., *Astroparticle Physics*, **89**, 57–65 (2017).
  - [2] Pasquale Dario Serpico, S Esposito, F Iocco, G Mangano, Gennaro Miele, and Ofelia Pisanti, *Journal of Cosmology and Astroparticle Physics*, **2004**(12), 010 (2004).
  - [3] Y al Xu, Kohji Takahashi, Stephane Goriely, Marcel Arnould, Masahisa Ohta, and Hiroaki Utsunomiya, *Nuclear Physics A*, **918**, 61–169 (2013).
  - [4] Koji Arai, D Baye, and Pierre Descouvemont, *Nuclear Physics A*, **699**(3-4), 963–975 (2002).
  - [5] L Lamia, C Spitaleri, RG Pizzone, E Tognelli, A Tumino, Scilla Degl’Innocenti, PG Prada Moroni, M La Cognata, L Pappalardo, and ML Sergi, *The Astrophysical Journal*, **768**(1), 65

- (2013).
- [6] O Fiedler and P Kunze, Nuclear Physics A, **96**(3), 513–520 (1967).
- [7] C Spitaleri, Recent applications of the trojan horse method in nuclear astrophysics, In *Exotic Nuclei And Nuclear/Particle Astrophysics*, pages 316–323. World Scientific (2006).
- [8] F Hammache, M Heil, S Typel, D Galaviz, K Sümmerer, A Coc, F Uhlig, F Attallah, M Caa-  
mano, D Cortina, et al., Physical Review C, **82**(6), 065803 (2010).
- [9] AM Mukhamedzhanov, LD Blokhintsev, and BF Irgaziev, Physical Review C, **83**(5), 055805  
(2011).
- [10] EM Tursunov, AS Kadyrov, SA Turakulov, and Igor Bray, Physical Review C, **94**(1), 015801  
(2016).
- [11] EM Tursunov, SA Turakulov, AS Kadyrov, and Igor Bray, Physical Review C, **98**(5), 055803  
(2018).
- [12] AM Mukhamedzhanov, RP Schmitt, Robert E Tribble, and A Sattarov, Physical Review C,  
**52**(6), 3483 (1995).
- [13] FE Cecil, Jingsheng Yan, and Cynthia S Galovich, Physical Review C, **53**(4), 1967 (1996).
- [14] K Langanke, Nuclear Physics A, **457**(2), 351–366 (1986).
- [15] KM Nollett, RB Wiringa, and R Schiavilla, Physical Review C, **63**(2), 024003 (2001).
- [16] EM Tursunov, SA Turakulov, and Pierre Descouvemont, Physics of Atomic Nuclei, **78**, 193–  
200 (2015).
- [17] Ali Kharbach and Pierre Descouvemont, Physical Review C, **58**(2), 1066 (1998).
- [18] R GH Robertson, P Dyer, RA Warner, RC Melin, TJ Bowles, AB McDonald, GC Ball,  
WG Davies, and ED Earle, Phys. Rev. Lett.:(United States), **47**(26) (1981).
- [19] M Anders, D Trezzi, R Menegazzo, M Aliotta, A Bellini, D Bemmerer, C Brogгинi, A Caciolli,  
P Corvisiero, H Costantini, et al., Physical Review Letters, **113**(4), 042501 (2014).
- [20] P Mohr, V Kölle, S Wilmes, U Atzrott, G Staudt, JW Hammer, H Krauss, and H Oberhum-  
mer, Physical Review C, **50**(3), 1543 (1994).
- [21] J Kiener, HJ Gils, H Rebel, S Zagromski, G Gsottschneider, N Heide, H Jelitto, J Wentz, and  
G Baur, Physical Review C, **44**(5), 2195 (1991).
- [22] SB Igamov and R Yarmukhamedov (1999).
- [23] S Typel, G Bläge, and K Langanke, Zeitschrift für Physik A Hadrons and Nuclei, **339**, 335–339  
(1991).

- [24] NA Burkova, KA Zhaksibekova, MA Zhusupov, and RA Eramzhyan, *Physics Letters B*, **248**(1-2), 15–20 (1990).
- [25] GG Ryzhikh, RA Eramzhyan, and S Shlomo, *Physical Review C*, **51**(6), 3240 (1995).
- [26] HW Hammer, Chen Ji, and DR Phillips, *Journal of Physics G: Nuclear and Particle Physics*, **44**(10), 103002 (2017).
- [27] Emil Ryberg, *Cluster effective field theory*, (Chalmers Tekniska Hogskola (Sweden), 2016).
- [28] Kai Siegbahn, *Alpha-, beta-and gamma-ray spectroscopy*, (Elsevier, 2012).
- [29] Masatsugu Sei Suzuki (2015).
- [30] Farzaneh Nazari, Mahdi Radin, and M Moeini Arani, *The European Physical Journal A*, **59**(2), 20 (2023).
- [31] Renato Higa, Gautam Rupak, and Akshay Vaghani, *The European Physical Journal A*, **54**, 1–12 (2018).
- [32] J Braun, W Elkamhawy, R Roth, and HW Hammer, *Journal of Physics G: Nuclear and Particle Physics*, **46**(11), 115101 (2019).
- [33] Mavrin L Goldberger and Kenneth M Watson, INC. New York-London-Sydney (1964).
- [34] Xinwei Kong and Finn Ravndal, *Nuclear Physics A*, **665**(1-2), 137–163 (2000).
- [35] Barry R Holstein, *Physical Review D*, **60**(11), 114030 (1999).
- [36] R Higa, H-W Hammer, and U van Kolck, *Nuclear Physics A*, **809**(3-4), 171–188 (2008).
- [37] Shung-Ichi Ando, *The European Physical Journal A*, **52**(5), 130 (2016).
- [38] HA Bethe, *Physical Review*, **76**(1), 38 (1949).
- [39] Shung-ichi Ando, Jae Won Shin, Chang Ho Hyun, and Seung-Woo Hong, *Physical Review C*, **76**(6), 064001 (2007).
- [40] David B Kaplan, Martin J Savage, and Mark B Wise, *Nuclear Physics B*, **534**(1-2), 329–355 (1998).
- [41] Milton Abramowitz and Irene A Stegun, *Handbook of mathematical functions* (1972).
- [42] Shung-Ichi Ando, *The European Physical Journal A*, **57**(1), 17 (2021).
- [43] Shung-Ichi Ando, *Physical Review C*, **100**(1), 015807 (2019).
- [44] Xinwei Kong and Finn Ravndal, *Physical Review C*, **64**(4), 044002 (2001).



